Nitrogen-vacancy defects in germanium

Cite as: AIP Advances **12**, 045110 (2022); https://doi.org/10.1063/5.0080958
Submitted: 05 December 2021 • Accepted: 18 March 2022 • Published Online: 06 April 2022

Navaratnarajah Kuganathan, Robin W. Grimes and Alexander Chroneos

Nitrogen-vacancy defects in germanium

Cite as: AIP Advances 12, 045110 (2022); doi: 10.1063/5.0080958
Submitted: 5 December 2021 • Accepted: 18 March 2022 •
Published Online: 6 April 2022

Navaratnarajah Kuganathan,[1,2,a] Robin W. Grimes,[1] and Alexander Chroneos[1,3]

AFFILIATIONS

[1] Department of Materials, Imperial College, London SW7 2AZ, United Kingdom
[2] Faculty of Engineering, Environment and Computing, Coventry University, Priory Street, Coventry CV1 5FB, United Kingdom
[3] Department of Electrical and Computer Engineering, University of Thessaly, 38221 Volos, Greece

[a] **Author to whom correspondence should be addressed:** n.kuganathan@imperial.ac.uk

ABSTRACT

While nitrogen doping has been investigated extensively in silicon, there is only limited information on its interaction with vacancies in germanium, despite most point defect processes in germanium being vacancy controlled. Thus, spin polarized density functional theory calculations are used to examine the association of nitrogen with lattice vacancies in germanium and for comparison in silicon. The results demonstrate significant charge transfer to nitrogen from the nearest neighbor Ge and strong N–Ge bond formation. The presence of vacancies results in a change in nitrogen coordination (from tetrahedral to trigonal planar) though the total charge transfer to N is maintained. A variety of nitrogen vacancy clusters are considered, all of which demonstrated strong binding energies. Substitutional nitrogen remains an effective trap for vacancies even if it has already trapped one vacancy.

I. INTRODUCTION

The advent of high-k dielectrics has enabled better use of materials, such as Ge and silicon–germanium ($Si_{1-x}Ge_x$), for microelectronics devices.[1–3] However, while Ge is isostructural with Si, there exist important differences between the two materials.[4,5] These differences are reflected in the defect processes, which in turn impact the design and performance of devices.[6–8]

The presence of nitrogen (N) in Si has been examined previously as it can lock dislocations and thereby increase the mechanical strength of wafers.[9] Good mechanical properties are important when Si wafers are used for ultra-large-scale integration technologies as they must undergo numerous processing steps without breaking. Additionally, N in Si reduces voids and microdefects, such as A-swirls and D-defects, during crystal growth via the float-zone method,[10,11] and it suppresses the negative effect of metal contaminants.[12] Nitrogen-vacancy (NV) defect centers in Si, Ge, Sn, and Pb have potential application in current technologies, including sensors, bio-imaging, and thermometery at nanoscale.[13–17]

In Si, N atoms will readily interact with vacancies limiting the formation of the vacancy-oxygen defect (*V*O or A-center).[18] Nevertheless, under equilibrium conditions, the interaction of N with vacancies will not be significant as the concentration of vacancies is very low.[19] Nitrogen-vacancy defects do become relevant under non-equilibrium conditions (such as irradiation) where there can be a supersaturation of vacancies. In Ge, the situation is different as the vacancy is the dominant intrinsic point defect that facilitates the diffusion of most technologically important dopants.[20–23] Although N is a group V element, it is not an appropriate *n*-type dopant. However, while previous density functional theory (DFT) work has shown that N can interact with vacancies to form strongly bound N_mV_n defects in Ge,[24,25] there has been no thorough investigation of the electronic properties of these defects.

In this study, we employ density functional theory (DFT) calculations to identify minimum energy nitrogen-vacancy configurations and associated charge transfer in Ge and to enable direct comparison to Si.

II. COMPUTATIONAL METHODS

The plane wave DFT code VASP (Vienna *Ab* Initio Simulation Package)[26] was used to perform all calculations. This code uses projected augmented wave (PAW) pseudopotentials[27] to solve standard Kohn–Sham equations. A plane wave basis set with a cut-off of 500 eV was used in all calculations. Bulk and doped structures were modeled using 8 × 8 × 8 and a 4 × 4 × 4 Monkhorst–Pack[28] *k*-point meshes, respectively. A supercell containing 250 atoms was

employed to model doped configurations. The exchange–correlation energy term was described using the generalized gradient approximation (GGA) as modeled by Perdew, Burke, and Ernzerhof (PBE).[29] The conjugate gradient algorithm[30] was used to optimize both bulk and defect structures. In all relaxed configurations, forces on the atoms were less than 0.001 eV/Å. The effective charges on the atoms closer to the defect configurations were calculated using the Bader charge analysis.[31] We used the orbital dependent Coulomb potential (Hubbard U) and the exchange parameter J, as described by Dudarev *et al.*,[32] to describe the behavior of the localized *p* states of Ge, with values of U = 0 eV and J = 3.33 eV as reported previously.[33] Short range dispersive attractive forces were modeled using the zero damping DFT + D3 scheme as implemented by Grimme *et al.*[34]

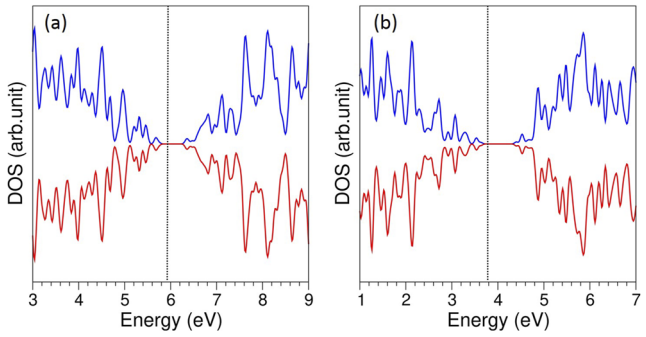

FIG. 1. DOS plots of bulk (a) Si and (b) Ge. The vertical black dotted lines correspond to the Fermi energy level.

III. RESULTS AND DISCUSSION

A. Structural modeling of Ge, Si, Si_3N_4, and Ge_3N_4

The starting point of this study was to demonstrate a good correlation between the predicted and experimentally determined crystal structures of cubic Si and Ge (space group $Fd\bar{3}m$, No : 227),[35,36] cohesive energies,[37,38] bandgap,[39,40] and bulk modulus[37,41] values by performing full geometry optimization calculations using the basis sets and pseudopotentials described earlier (see Table I). In Table II, we provide the calculated and experimental lattice parameters of α (and β)-Si_3N_4[42,43] and α (and β)-Ge_3N_4.[44,45] Total energies of α and β forms were calculated. The lowest energy structure was calculated for the α form for both Si_3N_4 and Ge_3N_4 although the energy difference is very small.

Cohesive energies of Si and Ge were calculated using the following equation:

$$E_{coh}(X = Si \text{ or } Ge) = E_X^{isolated} - E_X^{bulk}, \quad (1)$$

where $E_X^{isolated}$ and E_X^{bulk} are the total energies of an isolated gas phase X atom and the X atom in the bulk, respectively.

The calculated density of states (DOS) plots of bulk Si and Ge are shown in Figs. 1(a) and 1(b) with semiconducting bandgaps of 0.60 and 0.70 eV, respectively. While the predicted bandgap calculated for Si is smaller than the experimental value of 1.17 eV,[39] it is in good agreement with typical values (0.60, 0.61, and 0.71 eV) obtained from other DFT calculations.[46,47] The bandgap calculated for Ge is in excellent agreement with the experimental values.[40] In a previous simulation study,[48] we have shown that the absence of a U-J parameter would yield a much smaller bandgap value than the experimental value. In the optimized structure of N_2 molecule, the N–N bond distance is 1.11 Å, agreeing well with an experimental value of 1.09 Å.[49]

TABLE I. Calculated lattice parameters, cohesive energies, and bandgaps for Si and Ge. The corresponding experimental values are also provided. The values reported in the parentheses are for calculations without U parameter in bulk Ge.

	This study	Experiment	This study	Experiment
Parameter	Si		Ge	
a = b = c (Å)	5.45	5.43[35]	5.59 (5.76)	5.66[36]
E_{coh} (eV/atom)	4.73	4.63[37]	3.70 (3.86)	3.85[38]
E_{gap} (eV)	0.60	1.17[39]	0.70 (0.00)	0.74[40]
Bo (Mbar)	0.87	0.99[37]	0.84 (0.58)	0.75[41]

TABLE II. Calculated lattice parameters of bulk Si_3N_4 and Ge_3N_4 structures together with their corresponding experimental values. The relative energies per formula unit (f.u) calculated are also provided.

	This study	Experiment[42]	This study	Experiment[43]	This study	Experiment[44]	This study	Experiment[45]
Parameter	α-Si_3N_4		β-Si_3N_4		α-Ge_3N_4		β-Ge_3N_4	
a = b (Å)	7.806	7.765	7.654	7.595	8.321	8.202	8.153	8.203
c (Å)	5.660	5.628	2.928	2.902	6.023	5.941	3.128	3.077
Relative energy/f.u (eV)	0.00		+0.04		0.00		+0.03	

B. N-doped Ge and Si

Figures 2(a) and 2(b) show the structures of a single substitutional N atom in Si and Ge, respectively. In the relaxed configurations, the four nearest neighbor atoms are symmetrically attracted by the N atom, thereby retaining a tetragonal coordination with the nearest neighbor atoms. In the NSi_4 tetrahedral unit, the N–Si bond lengths are shorter by 0.33 Å than the Si–Si bond lengths [see Fig. 2(c)]. The strong bonding between the N and the Si atoms is evidenced by the Bader charges on the N and adjacent Si atoms: the N atom gains 3.30 electrons from the nearest neighbor Si atoms [see Fig. 2(c)]. This is due to the higher electronegativity of N (3.07) than Si (1.74).[50] The ~3 positive charges are practically equally distributed on the four nearest neighbor Si atoms [see Fig. 2(c)].

In the case of Ge, the N–Ge bond distances are 0.28 Å shorter than the Ge–Ge bond distance [see Fig. 2(d)]. The shorter N–Ge bond distance is again due to the electronegativity difference between the N (3.07) and the Ge (2.02)[50] reflected in the −3.03 Bader charge on the N, slightly lower than that found on the N in the Si. The smaller Bader charge on N in Ge than N in Si is due to the smaller electronegativity difference (1.05) between N and Ge than between Si and N (1.33). The charge density maps show the bonding interaction between N and Si (or Ge) [see Figs. 2(e) and 2(f)]. The electron density plots localized around the N atom in Si and Ge are shown in Figs. 3(a) and 3(b), respectively. The presence of three electrons on N makes these doped configurations metallic [see Figs. 3(c) and 3(d)]. The states associated with the N appear in the valence bands and Fermi energy levels according to the atomic DOS plots of N [see Figs. 3(e) and 3(f)].

The substitution energies for a single N atom to replace a single M (M = Si or Ge) atom were calculated using the following equation:

$$E_{Sub} = E_{(N:M\_supercell)} + E_{(M)} - E_{(M:supercell)} - \frac{1}{2}E(N_2), \quad (2)$$

where $E_{(M:Si\_supercell)}$ is the total energy of a single N atom substitutionally doped in the supercell of M, $E_{(M:supercell)}$ is the total energy

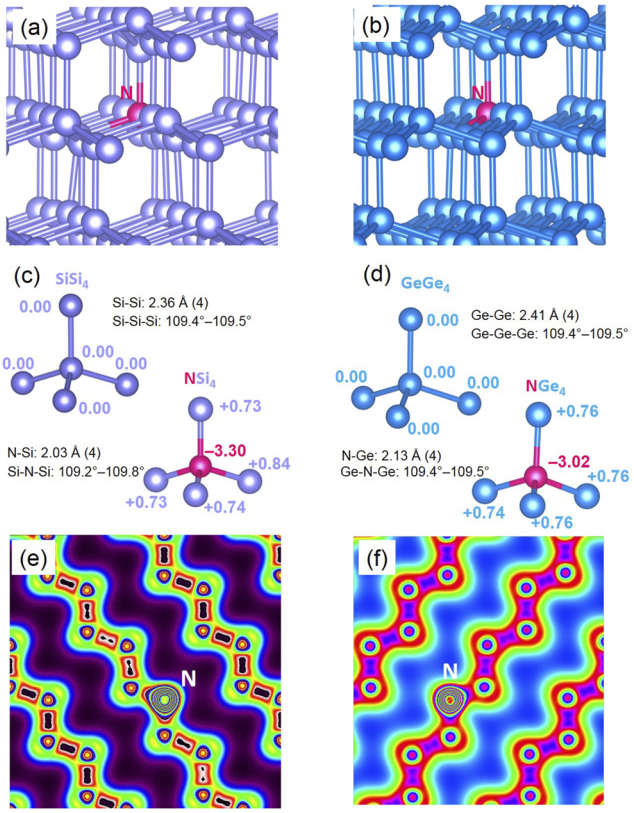

FIG. 2. Relaxed structures of (a) N-substituted Si and (b) N-substituted Ge. Tetrahedral units showing bond distances, bond angles, and the Bader charges in the relaxed configurations of (c) N-substituted Si and (d) N-substituted Si. Charge density plots showing the bonding interaction between (e) the N and Si and (f) the N and Ge.

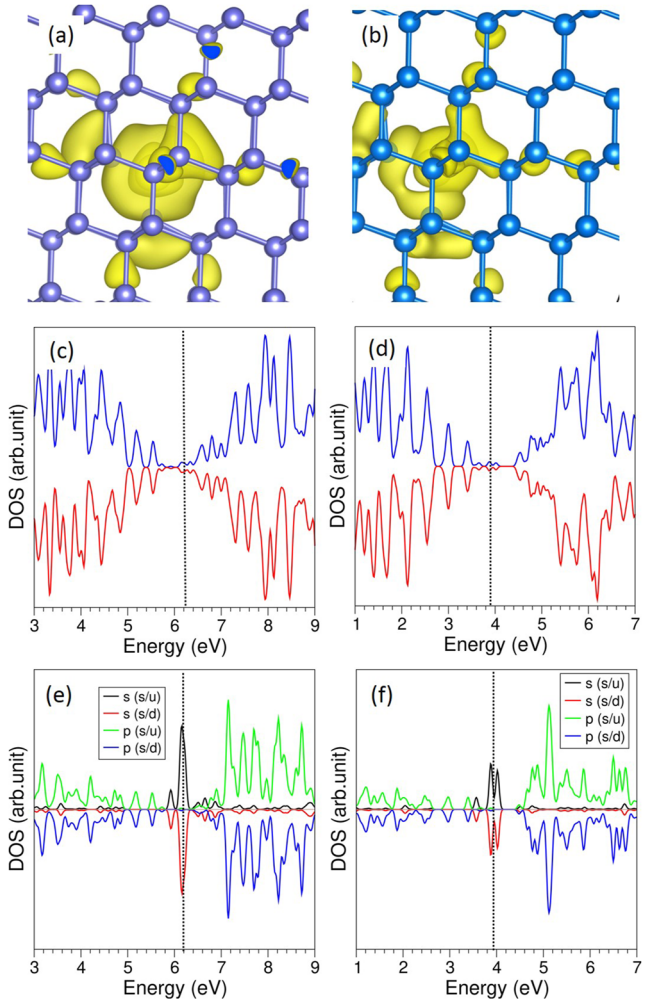

FIG. 3. Band-decomposed charge density plots of the N in (a) N-doped Si and (b) N-doped Ge. The corresponding total DOS plots (c) and (d) and atomic DOS plots of N (e and f) are also shown.

TABLE III. Calculated formation energies of point defects and defect clusters in Si and Ge.

Defect/defect cluster	Formation energy (eV) Si	Ge
V	3.51	3.13
N	0.50	1.59
VV	5.18	4.92
NN	−0.65	2.23
NV	1.40	1.53
N_2V	−3.62	−2.52
NV_2	−4.14	−3.13
N_2V_2	−4.99	−3.75

of the defect free supercell of M, $E_{(M)}$ is the energy of a M atom in its bulk, and $E(N_2)$ is the total energy of a N_2 molecule.

The calculated energies for the Si and Ge are 0.50 and 1.59 eV, respectively (see Table III). This indicates that the substitution of N in Si is a lower energy process than in Ge, a consequence of the strength of Si–N bonds compared to Si–Si bonds than Ge–N bonds are compared to Ge–Ge (see Fig. 2).

The energy to incorporate a single N atom on the pre-existing Si (or Ge) vacancy defect was calculated according to the following equation:

$$E_{Inc} = E_{(N:M\_supercell)} - E_{V_M:supercell} - \frac{1}{2}E(N_2), \quad (3)$$

where $E_{V_M:supercell}$ is the total energy of a supercell containing a vacant M (M = Si or Ge) site. The incorporation energy onto a V_{Si} is −3.01 eV consistent with it being energetically favorable for $\frac{1}{2}N_2$ to dissociate and occupy the Si vacancy if a vacancy is readily available. This is because the pre-existing electrons in the defect lattice facilitate the incorporation of N via charge transfer. In the case of Ge, the incorporation energy is −1.59 eV. The lower exoergic incorporation for Ge is due to the weaker bonding between the N and the Ge compared to N and the Si.

C. NN and VV defect pairs

This report is concerned with the stability and electronic structure of defects formed when substitutional N species bind to vacancies. These heteronuclear clusters will be in competition with homonuclear clusters formed when two N substitutional defects form a NN cluster pair or two vacancies form a VV cluster.

Figure 4(a) shows the structure of the most stable arrangement of two vacancies in Si. A similar configuration was also calculated for Ge [see Fig. 4(c)]. In both cases, the vacancies are in nearest neighbor positions. This is in good agreement with previous studies, which also predict the preference for a nearest neighbor arrangement.[24] Following Eq. (2), the formation energies of a VV cluster in Si and Ge are 5.18 and 4.92 eV, respectively (see Table III).

Figures 4(b) and 4(d) show the structures of the most stable NN cluster in Si and Ge, respectively. Both N remain on Si (or Ge) sites, which are in nearest neighbor positions. This agrees with a previous DFT simulation.[24] Again, following Eq. (2), the energies to form the NN di-substitution cluster in Si and Ge are −0.65 and 2.23 eV, respectively (see Table III). That means the solution of $\frac{1}{2}N_2$ is exothermic. However, N_2 reacts with Si to form Si_3N_4 solid. If this is taken as the reference state, the solution of Si_3N_4 into Si is endothermic with a value of +2.99 eV.

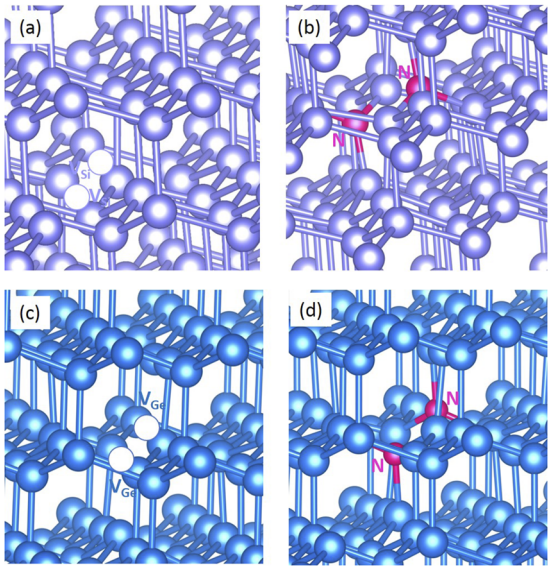

FIG. 4. Most stable relaxed structures of (a) di-vacancy cluster (VV) and (b) NN di-substituted cluster in Si. The corresponding structures [(c) and (d)] obtained for Ge are also shown.

To determine the stability of the cluster with respect to isolated species, the cluster binding energy is predicted. This is calculated via

$$E_{Binding}(NN) = 2E_{Sub}(NN) - 2E_{Sub}(N), \quad (4)$$

which implies that, if the binding energy is negative, the cluster is stable.

The binding energy for the VV cluster in Si is −1.84 eV and in Ge −1.34 eV. The binding energy for the NN cluster in Si is −1.65 eV and in Ge −0.95 eV. Thus, all four binary clusters are stable with respect to their isolated components.

D. NV defects

Next calculations were performed for a single substitutional N atom in Si (or Ge) at sites adjacent to a pre-existing Si (or Ge) vacancy. The relaxed structures are shown in Figs. 5(a) and 5(b). Different NV defect configurations were considered. Their structures and relative energies are provided in the supplementary material. The lowest energy configuration, in which N and vacancy are nearest neighbors, was considered for further analysis.

The substitutional N atom in Si relaxes from perfect tetrahedral symmetry to form a distorted trigonal planar structure with three identical bond angles of 117.8° and three Si–N bond lengths of 1.84 Å. There is a significant reduction (by ~0.20 Å) in the Si–N bond distances compared to those calculated in the absence of the Si vacancy [compare Figs. 2(c) and 5(c)]. The strong bonding between the N and Si atoms is confirmed by the higher positive Bader charges (~+1.00) on the Si atoms [Fig. 5(c)] than that calculated (~+0.76) in

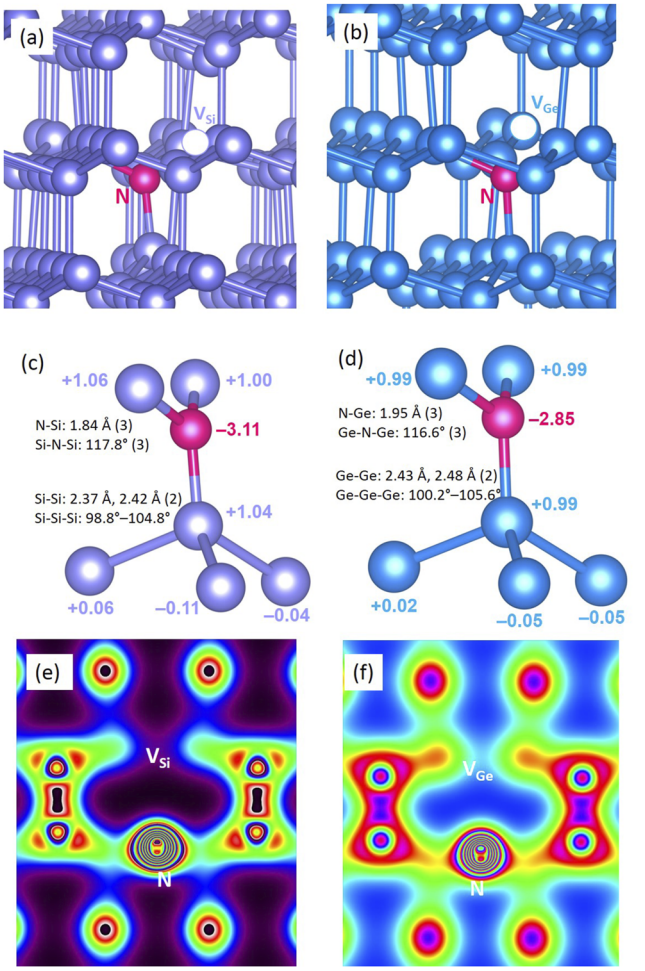

FIG. 5. Relaxed structures of a single N atom substitutionally doped on the (a) Si site and (b) Ge site in the presence of a vacancy closer to the dopant. Bond distances, bond angles, and the Bader charges closer to the dopant in the relaxed configurations of (c) N-substituted Si and (d) N-substituted Si. Charge density plots associated with the (e) N_{Si}–V_{Si} and (f) N_{Ge}–V_{Ge} pairs.

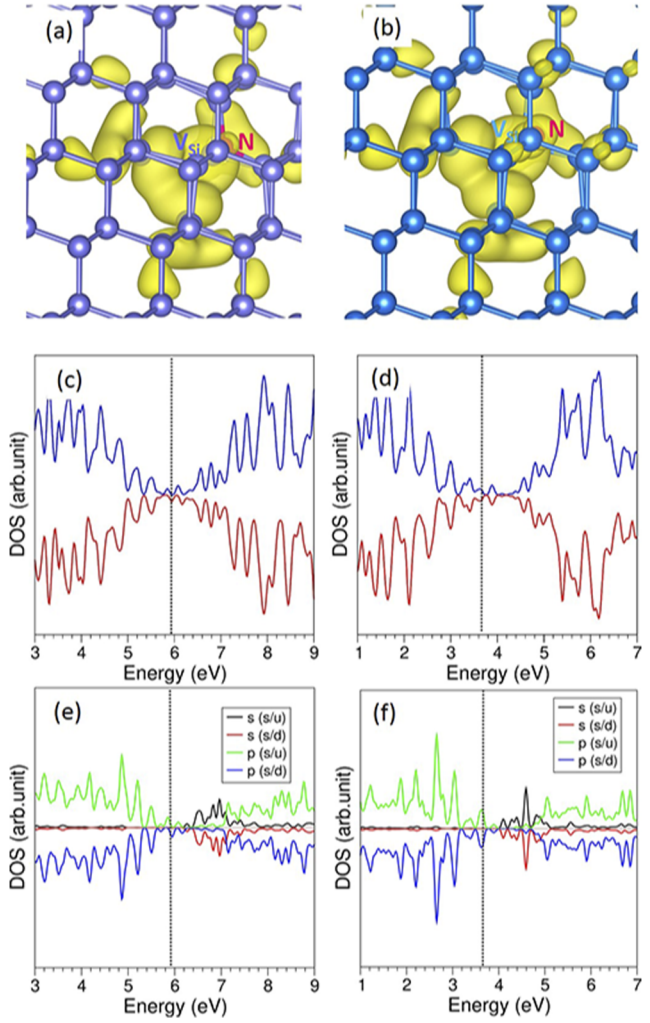

FIG. 6. Band-decomposed charge density plot around the N atom in the (a) N_{Si}–V_{Si} and (b) N_{Ge}–V_{Ge} clusters. The corresponding total DOS plots (c) and (d) and atomic DOS plots of N (e) and (f) are also shown.

the absence of a Si vacancy [Fig. 2(c)]. That is, the N atom still gains approximately three electrons to complete its 2p shell but now from the three Si atoms to which it is bonded.

In the case of Ge, the Bader charge on the N in the NGe_3 unit is −2.85, slightly lower than that calculated on the N in the NSi_3 unit, again reflecting the higher electronegativity of Ge than Si (but still practically completing the N outer p shell). The N–Ge bond distance is longer than the N–Si bond distance [see Figs. 5(c) and 5(d)]. This is primarily due to the larger atomic radius of Ge than Si. The bond angles in the NGe_3 unit are very close to those calculated in the NSi_3 unit. The charge density plots show the interaction between the N atom and the nearest neighbor atoms [see Figs. 5(e) and 5(f)].

The local charge density around the N atom in the relaxed configurations is shown in Figs. 6(a) and 6(b). The total DOS plots show that the resultant structures are metallic [see Figs. 6(c) and 6(d)]. This can be partly due to the electrons arising from the vacancy in the lattice. The atomic DOS plots calculated for N show that *p*-states are strongly localized in the valence bands and the Fermi levels [see Figs. 6(e) and 6(f)].

The vacancy formation energies were calculated in the absence and presence of N doping. In the undoped Si and Ge lattices, the vacancy formation energies are 3.51 and 3.13 eV, respectively (see Table III), agreeing well with previous calculations.[51,52] Adjacent to a pre-existing N substitutional atom, these values drop to 1.41 and 1.53 eV. Thus, N doping facilitates the formation of a Si vacancy by 2.10 eV and a Ge vacancy by 1.60 eV.

The cluster binding energies were calculated from isolated substitutional N and an isolated vacancy but also from NN and VV di-clusters (which demands the dissociation of these clusters). From isolated defects, the binding energies are of −2.10 and −1.60 eV for the formation of N_{Si}–V_{Si} and N_{Ge}–V_{Ge} clusters, respectively,

meaning that there is a strong driving force for cluster formation. From di-clusters, the binding energies are reduced to −0.37 eV in Si and −0.43 eV in Ge. This means that while the VV defects are strongly bound, N will still preferentially associate with vacancies in both Si and Ge. That is, as long as the concentration of nitrogen substitutional defects is higher than that of vacancies, it will strongly depress the concentration of the isolated vacancies or VV clusters by forming the NV clusters (and vice versa, that is, if the V concentration is higher than N substitutional, it will suppress the concentration of isolated N). This offers the possibility that V or VV cluster mobility may be negatively impacted by the presence of substitutional N species and thus also the transport of dopants that rely on a V or VV mediated mechanism, though further work is needed to identify a mechanistic basis for this.

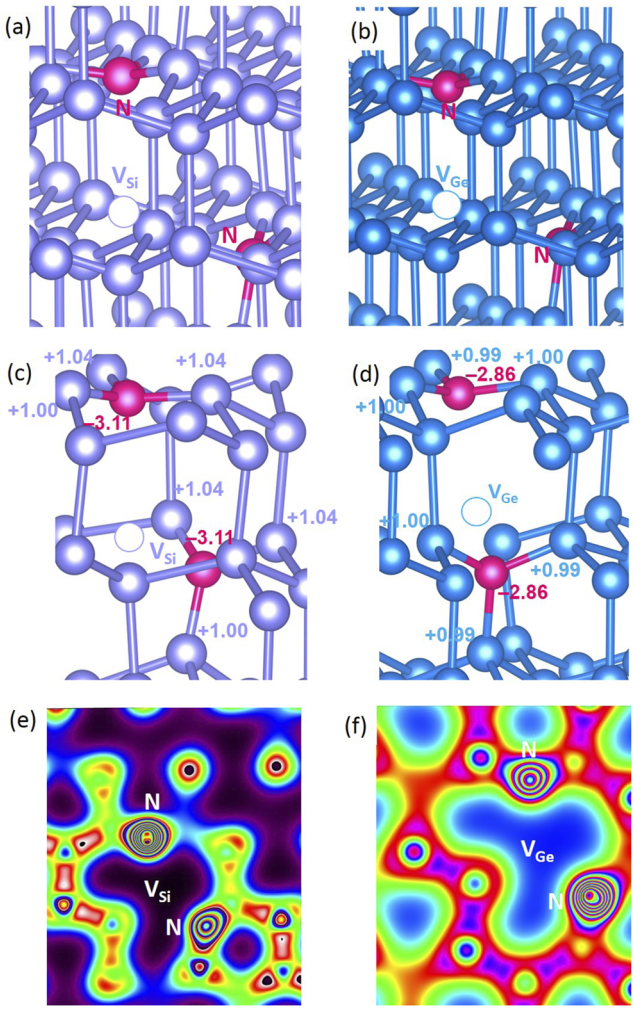

FIG. 7. Relaxed structures of two N atoms substitutionally doped on the (a) Si and (b) Ge site in the presence of a nearest neighbor vacancy. Bond distances, bond angles, and Bader charges around the dopants in the (c) N_{Si}–V_{Si}–N_{Si} and (d) N_{Ge}–V_{Ge}–N_{Ge} clusters. Charge density plots associated with the (e) N_{Si}–V_{Si}–N_{Si} and (f) N_{Ge}–V_{Ge}–N_{Ge} clusters.

E. N_2V defects

The next nitrogen vacancy combination considered consisted of two substitutional N atoms adjacent to a single nearest neighbor Si (or Ge) vacancy (i.e., N_{Si}–V_{Si}– N_{Si} or N_{Ge}–V_{Ge}–N_{Ge}). The relaxed structures are shown in Figs. 7(a) and 7(b), indicating that the N substitutional species form a bent configuration with the vacancy. We have considered other N_2V defect configurations with higher total energy than that calculated for the configuration reported here (see the supplementary material). Each N atom forms a three coordinated structure with three nearest neighbor Si (or Ge) atoms. The N–Si (or Ge) bond lengths and bond angles are almost the same as the values predicted for the N_{Si}–V_{Si} and N_{Ge}–V_{Ge} configurations [see Figs. 7(c) and 7(d)]. The Bader charge on each N atom in the NSi_3 unit is −3.11 again essentially taking a single electron from each of the adjacent three Si atoms. In the case of Ge, a lower negative charge of −2.86 is predicted on the N atoms. The charge density

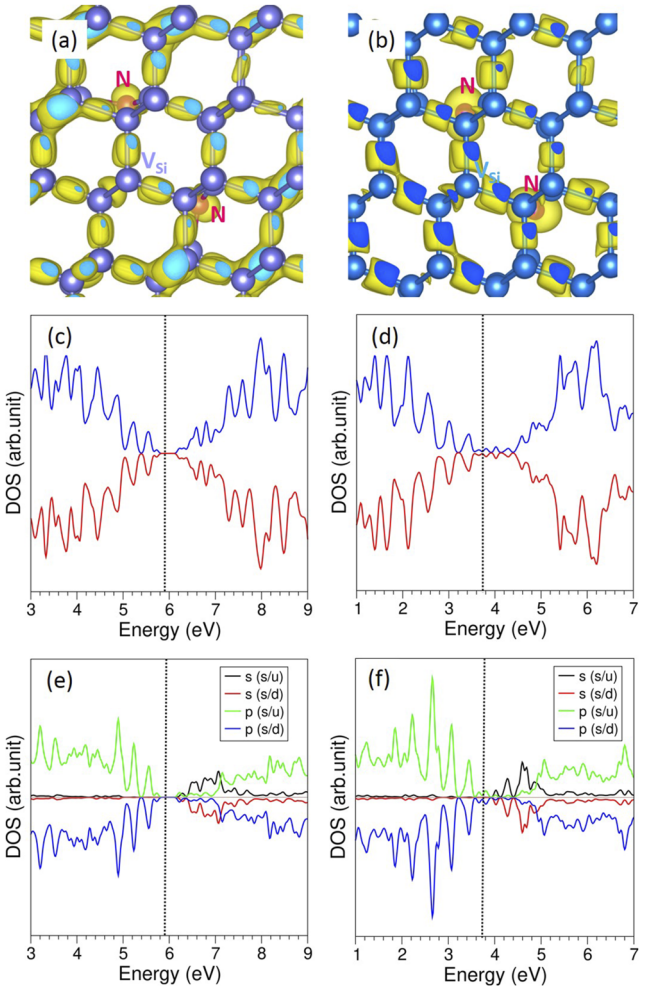

FIG. 8. Band-decomposed charge density plots around the N atoms in the (a) N_{Si}–V_{Si}–N_{Si} and (b) N_{Ge}–V_{Ge}–N_{Ge} clusters. The corresponding total DOS plots (c) and (d) and atomic DOS plots of N (e) and (f) are also shown.

plots showing the interaction between the N atoms and the nearest neighbor atoms are presented in Figs. 7(e) and 7(f).

The band-decomposed charge density plots around the N atom indicate that the electrons are mainly localized on the N atoms, and there is a dispersion of charges throughout the lattice [see Figs. 8(a) and 8(b)]. The total DOS plot shows that the resultant doped configuration (N_{Si}–V_{Si}–N_{Si}) maintains a narrow gap [see Fig. 8(c)]. The *p* states of N are mainly localized in the valence band [see Fig. 7(e)]. Conversely, a metallic character is noted for the N_{Ge}–V_{Ge}–N_{Ge} configuration [see Figs. 8(d) and 8(f)].

The total binding energy to form the N_{Si}–V_{Si}–N_{Si} cluster from isolated defects ($2N_{Si}$ and V_{Si}) is −3.62 eV, inferring a strong preference to form the cluster (see Table III). The binding energy for the N_{Ge}–V_{Ge}–N_{Ge} cluster, while lower, −2.52 eV, is still substantial. The (binding) energies to associate a second substitutional N with N_{Si}–V_{Si} and N_{Ge}–V_{Ge} clusters to form N_{Si}–V_{Si}–N_{Si} or N_{Ge}–V_{Ge}–N_{Ge} clusters are 1.52 and 0.92 eV, respectively. These binding energies indicate there is still a substantial driving force for the association of a second N substitutional atom with the NV di-cluster.

Considering the formation from VV and NN clusters, the total binding energies drop to −1.07 eV in Si and −0.90 eV in Ge, still indicating strong association. Following this, if we consider association of a second N with an existing N–V cluster from the dissociation of the N_{Si}–N_{Si} (or N_{Ge}–N_{Ge}) cluster, the energy is still exothermic (0.69 and 0.19 eV in Si and Ge, respectively). Thus, if there are sufficient nitrogen substitutional species, two N will bind to a vacancy. This may further impact transport of dopants through the lattice if it leads to a mechanism to further inhibit vacancy mobility.

F. NV_2 defects

The next cluster investigated consisted of two vacancies adjacent to a substitutional N. Different configurations were considered (see the supplementary material), and the lowest energy configuration is reported here. The relaxed structures show the formation of a distorted planar configuration (NSi_3 and NGe_3) [see Figs. 9(a) and 9(b)] as described for the single vacancy and double N clusters above. The bond distances and angles in these planar structures are almost identical with those found in the NV and N_2V defects.

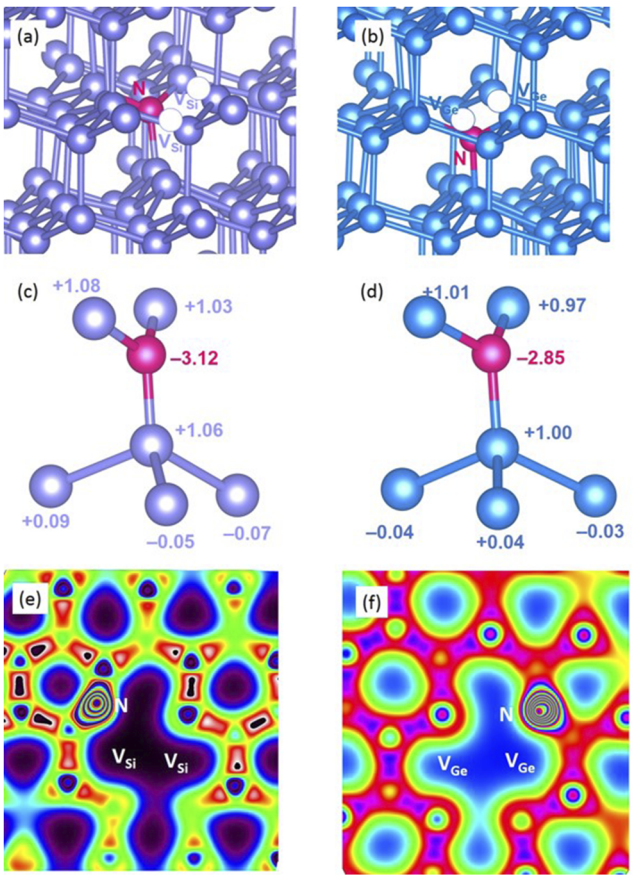

FIG. 9. Relaxed structures of a single N atom substitutionally doped on the (a) Si site and (b) Ge site in the presence of two vacancies closer to the dopant. Bader charges closer to the dopant in the relaxed configurations of (c) N-substituted Si and (d) N-substituted Ge. Charge density plots associated with the (e) N_{Si}–V_{Si}–V_{Si} and (f) N_{Ge}–V_{Ge}–V_{Ge} pairs.

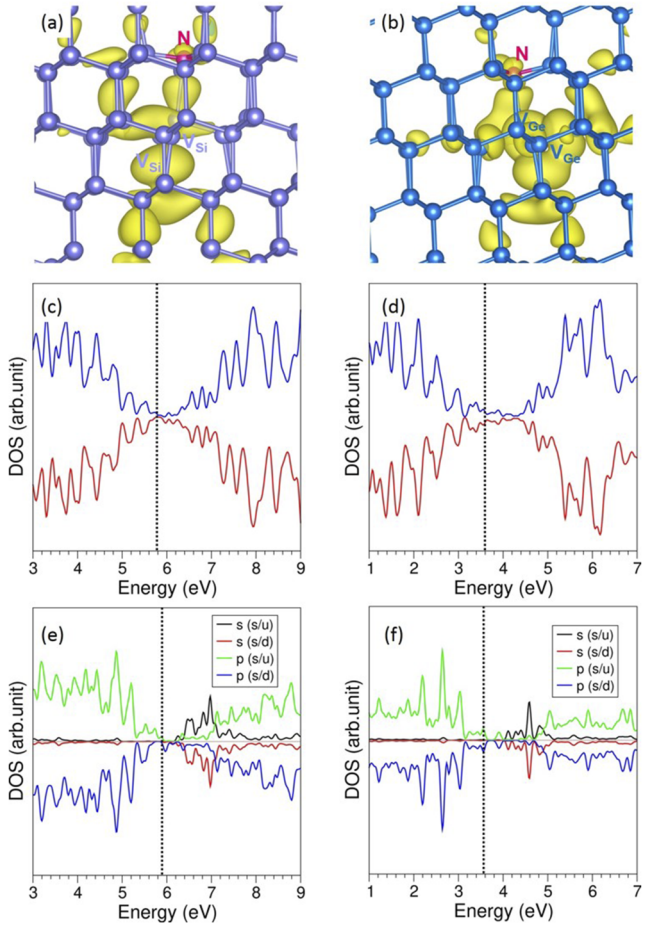

FIG. 10. Band-decomposed charge density plots around the N atoms in the (a) N_{Si}–V_{Si}–V_{Si} and (b) N_{Ge}–V_{Ge}–V_{Ge} clusters. The corresponding total DOS plots (c) and (d) and atomic DOS plots of N (e) and (f) are also shown.

Again, almost complete N p-shells are predicted, the Bader charges of −3.12 and −2.85 for NSi_3 and NGe_3, respectively [see Figs. 9(c) and 9(d)]. The charge density plots show the interaction between the N substitutional species and the vacancies [see Figs. 9(e) and 9(f)].

According to the band-decomposed charge density plots, the electrons are mostly localized around the vacancies [see Figs. 10(a) and 10(b)]. The resultant configurations exhibit metallic character [Figs. 10(c) and 10(d)]. The Fermi energy levels have a small contribution from the *p* states of N [Figs. 10(e) and 10(f)].

The predicted total binding energies to form the N_{Si}–V_{Si}–V_{Si} cluster from isolated defects (2 V_{Si} and N_{Si}) are −4.14 eV and, in correspondence with previous results, a lower binding energy of −3.13 eV for the N_{Ge}–V_{Ge}–V_{Ge} cluster. If we consider the formation of the clusters from NN and VV clusters, the binding energies are −1.48 eV in Si and −1.31 eV in Ge, still indicating strong association. The formation of these clusters was also considered from a vacancy (V_{Si} or V_{Ge}) and a N_{Si}–V_{Si} (or N_{Ge}–V_{Ge}) cluster with favorable binding energies predicted of −2.02 eV for N_{Si}–V_{Si}–V_{Si} and −1.47 eV for N_{Ge}–V_{Ge}–V_{Ge}. Interestingly, these values are almost the same as the binding energies to form the pair N_{Si}–V_{Si} (or N_{Ge}–V_{Ge}) clusters: that is, the energy gained from association of the second vacancy is almost the same as that for the first vacancy. If the second vacancy is taken via the dissociation of a VV cluster, the association of the second vacancy is still exothermic with an energy of 0.82 eV in Si and 0.61 eV in Ge. These energies all indicate a greater association of a V with a cluster containing a N than association of a second N (compared to values in Sec. III D). That means a nitrogen substitutional species remains an effective trap for a vacancy (including via VV cluster dissociation) even if it has already trapped one vacancy. Thus, the nitrogen substitutional species may impact the transport of dopants through the lattice even if there are more vacancies than nitrogen (though the mechanism needs to be identified).

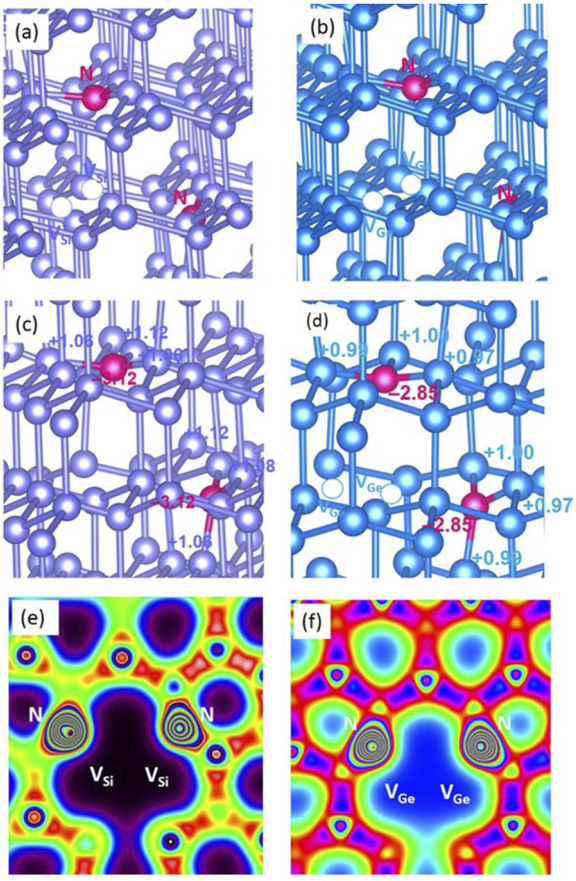

FIG. 11. Relaxed configurations of (a) N_{Si}–V_{Si}–V_{Si}–N_{Si} and (b) N_{Ge}–V_{Ge}–V_{Ge}–N_{Ge} cluster. Bader charges around the N atoms in (c) N_{Si}–V_{Si}–V_{Si}–N_{Si} and (d) N_{Ge}–V_{Ge}–V_{Ge}–N_{Ge} cluster. The corresponding charge density plots (e) and (f) are also shown.

G. N_2V_2 defects

Finally, structures were predicted resulting from two substitutional N atoms in the presence of two Si (Ge) vacancies (i.e., four- or

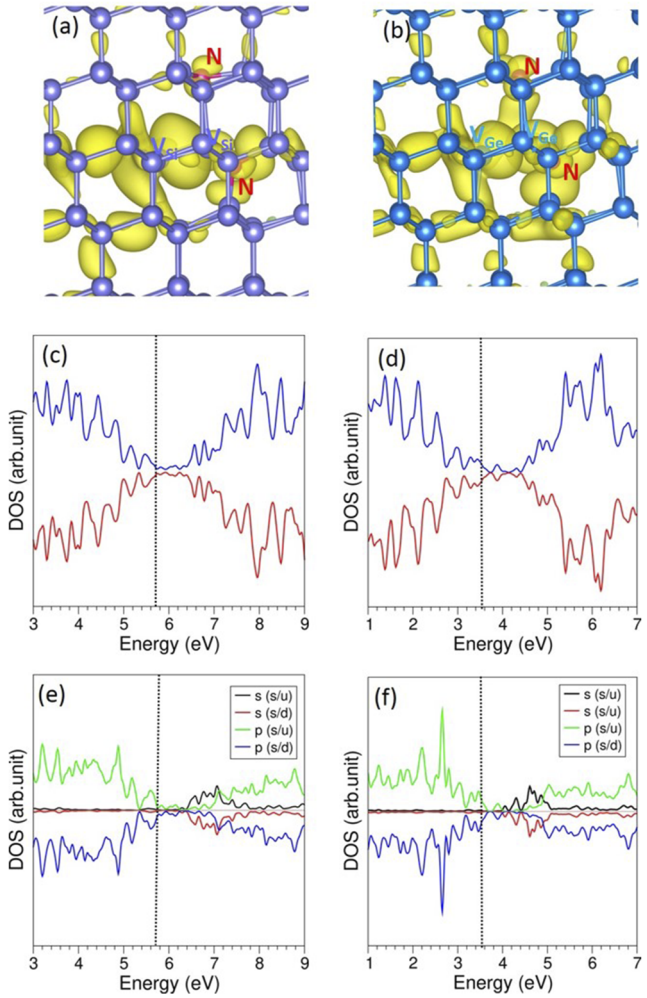

FIG. 12. Band-decomposed charge density plots around the N atoms in (a) N_{Si}–V_{Si}–V_{Si}–N_{Si} and (b) N_{Ge}–V_{Ge}–V_{Ge}–N_{Ge} cluster. The corresponding total DOS plots (c) and (d) and atomic DOS plots (e) and (f) are also shown.

TABLE IV. Binding energies calculated for the formation of N_{Si}–V_{Si}–V_{Si}–N_{Si} and N_{Ge}–V_{Ge}–V_{Ge}–N_{Ge} clusters.

Defect cluster formation process	Binding energy (eV)
N_{Si}–V_{Si} + N_{Si}–V_{Si} → N_{Si}–V_{Si}–V_{Si}–N_{Si}	−0.79
N_{Si}–V_{Si}–N_{Si} + V_{Si} → N_{Si}–V_{Si}–V_{Si}–N_{Si}	−1.37
N_{Si}–V_{Si}–V_{Si} + N_{Si} → N_{Si}–V_{Si}–V_{Si}–N_{Si}	−0.85
2 N_{Si} + 2 V_{Si} → N_{Si}–V_{Si}–V_{Si}–N_{Si}	−4.99
V_{Si}–V_{Si} + N_{Si}–N_{Si} →N_{Si}–V_{Si}–V_{Si}–N_{Si}	−1.52
N_{Ge}–V_{Ge} + N_{Ge}–V_{Ge} → N_{Ge}–V_{Ge}–V_{Ge}–N_{Ge}	−0.55
N_{Ge}–V_{Ge}–N_{Ge} + V_{Ge} → N_{Ge}–V_{Ge}–V_{Ge}–N_{Ge}	−1.23
N_{Ge}–V_{Ge}–V_{Ge} + N_{Ge} → N_{Ge}–V_{Ge}–V_{Ge}–N_{Ge}	−0.62
2 N_{Ge} + 2 V_{Ge} → N_{Ge}–V_{Ge}–V_{Ge}–N_{Ge}	−3.75
V_{Ge}–V_{Ge} + N_{Ge}–N_{Ge} → N_{Ge}–V_{Ge}–V_{Ge}–N_{Ge}	−1.46

tetra-defect cluster). The relaxed structures are shown in Figs. 11(a) and 11(b). Again, the Bader charge (−3.12) on each N was donated equally by three Si atoms (~1.05*e* from each Si) [see Fig. 11(c)]. Two adjacent distorted trigonal planar units (NSi_3) are formed each with similar structures predicted for other clusters. Shorter N–Si bonds (1.84 Å) confirm the strong bonding between N and Si. In the case of Ge, the Bader charge on each N atom is −2.85 [see Fig. 11(d)]. The cross-sectional charge density plots [Figs. 11(e) and 11(f)] show the bonding interaction between the N and Si in the NSi_3 unit and the N and Ge in the NGe_3 unit.

The electron density around the N atoms in the relaxed structures are shown in Figs. 12(a) and 12(b). The total DOS plot shows that the resultant structures are metallic [see Figs. 12(c) and 12(d)]. The atomic DOS plots of N are shown in Figs. 12(e) and 12(f). The Fermi energy levels are mainly localized with *p* states of N.

The binding energies were predicted for the formation of N_{Si}–V_{Si}–V_{Si}–N_{Si} and N_{Ge}–V_{Ge}–V_{Ge}–N_{Ge} clusters via different routes (see Table IV): in all cases, they are exothermic, and the energies for Si are universally greater than the energies for equivalent processes in Ge. The formation of the tetra-cluster from four isolated point defects is greater but not markedly greater than twice the energy to form two di-clusters (in Si, −4.99 eV compared to 4.20 eV). The energy to associate a N with a pre-existing N–V–V tri-cluster while exothermic is also not particularly high (0.85 eV for Si and 0.62 for Ge) whereas the energy to associate a V with a pre-existing N–N–V tri cluster is 1.37 eV for Si and 1.26 eV for Ge. This suggests, again, that vacancies exhibit stronger binding energies to form (small) clusters with N or nitrogen containing clusters than N does to cluster that already contain a N species. That is, the N substitutional species act to associate isolated vacancies.

IV. CONCLUSIONS

The structures and energetics of various nitrogen-vacancy defects in Ge have been predicted using atomic scale calculations based on DFT corrected for dispersion interactions. Vacancies are the dominant intrinsic defect in Ge. For comparison, the same calculations are reported for Si, aspects of which have been reported in previous studies.

We predict that N substitutional doping is accommodated by the formation of strong N–Ge (Si) bonds. There is significant charge transfer to the N from its nearest neighbors, which essentially completes its 2p shell. The presence of a vacancy leads to a change in N coordination number, from initially tetrahedral to trigonal planar (i.e., from 4 to 3), although the total charge transfer to the N atom remains roughly the same (i.e., it still completes the 3p shell).

The aggregation of isolated defects to form dopant-vacancy clusters, NV, NNV, NVV, and NNVV, is accompanied by strong favorable (exoergic) binding energies. Even the association of a second vacancy with a NV cluster is strongly favorable. Through this, the presence of substitutional N in Ge may degrade the efficacy of vacancy mediated processes responsible for the transport of dopants, since the vacancy transport is dominant in Ge (whereas the interstitial transport is more important in Si). The N doping process introduces gap states leading to band-gap narrowing, which can play a significant role in the performance of devices.

SUPPLEMENTARY MATERIAL

See the supplementary material for different configurations of NV, NV_2, N_2V, and N_2V_2 defects in Si and Ge.

ACKNOWLEDGMENTS

Computational facilities and support were provided by High Performance Computing Centre at Imperial College London.

AUTHOR DECLARATIONS

Conflict of Interest

The authors have no conflicts to disclose.

DATA AVAILABILITY

The data that support the findings of this study are available from the corresponding author upon reasonable request.

REFERENCES

[1] H. Kim, C. O. Chui, K. C. Saraswat, and P. C. McIntyre, Appl. Phys. Lett. **83**, 2647 (2003).
[2] F. Boscherini, F. D'Acapito, S. F. Galata, D. Tsoutsou, and A. Dimoulas, Appl. Phys. Lett. **99**, 121909 (2011).
[3] E. Shigesawa, R. Matsuoka, M. Fukumoto, R. Sano, K. M. Itoh, H. Nohira, and K. Sawano, Semicond. Sci. Technol. **33**, 124020 (2018).
[4] J. Vanhellemont and E. Simoen, J. Electrochem. Soc. **154**, H572–H583 (2007).
[5] E. Bruno, S. Mirabella, G. Scapellato, G. Impellizzeri, A. Terrasi, F. Priolo, E. Napolitani, D. De Salvador, M. Mastromatteo, and A. Carnera, Phys. Rev. B **80**, 033204 (2009).
[6] C. Claeys and E. Simoen, *Germanium-Based Technologies: From Materials to Devices* (Elsevier, Amsterdam, 2007).
[7] A. Chroneos and H. Bracht, Appl. Phys. Rev. **1**, 011301 (2014).
[8] A. Chroneos, E. N. Sgourou, C. A. Londos, and U. Schwingenschlögl, Appl. Phys. Rev. **2**, 021306 (2015).
[9] K. Sumino, I. Yonenaga, M. Imai, and T. Abe, J. Appl. Phys. **54**, 5016 (1983).
[10] H. Ishii, K. Oka, K. Motonami, T. Koyama, and J. Izumitani, Jpn J. Appl. Phys., Part 2 **35**, L1385 (1996).

[11] W. von Ammon, R. Hölzl, J. Virbulis, E. Dornberger, R. Schmolke, and D. Gräf, J. Cryst. Growth **226**, 19 (2001).
[12] F. Shimura and R. S. Hockett, Appl. Phys. Lett. **48**, 224 (1986).
[13] T. Plakhotnik and H. Aman, "NV-centers in nanodiamonds: How good they are," Diamond Relat. Mater. **82**, 87 (2018).
[14] M. W. Doherty, N. B. Manson, P. Delaney, F. Jelezko, J. Wrachtrup, and L. C. L. Hollenberg, "The nitrogen-vacancy colour centre in diamond," Phys. Rep. **528**, 1 (2013).
[15] R. Schirhagl, K. Chang, M. Loretz, and C. L. Degen, "Nitrogen-vacancy centers in diamond: Nanoscale sensors for physics and biology," Annu. Rev. Phys. Chem. **65**, 83 (2014).
[16] L. Rondin, J.-P. Tetienne, T. Hingant, J.-F. Roch, P. Maletinsky, and V. Jacques, "Magnetometry with nitrogen-vacancy defects in diamond," Rep. Prog. Phys. **77**, 056503 (2014).
[17] T. Plakhotnik, "Diamonds for quantum nano sensing," Curr. Opin. Solid State Mater. Sci. **21**, 25–34 (2017).
[18] E. N. Sgourou, T. Angeletos, A. Chroneos, and C. A. Londos, J. Mater. Sci.: Mater. Electron. **27**, 2054 (2016).
[19] A. Taguchi, H. Kageshima, and K. Wada, J. Appl. Phys. **97**, 053514 (2005).
[20] M. Werner, H. Mehrer, and H. D. Hochheimer, Phys. Rev. B **32**, 3930 (1985).
[21] R. Kube, H. Bracht, A. Chroneos, M. Posselt, and B. Schmidt, J. Appl. Phys. **106**, 063534 (2009).
[22] J. K. Prussing, G. Hamdana, D. Bougeard, E. Peiner, and H. Bracht, J. Appl. Phys. **125**, 085105 (2019).
[23] S. Dev, N. Pradhan, N. Variam, and S. Lodha, IEEE Trans. Electron Devices **67**, 419–423 (2020).
[24] A. Chroneos, J. Appl. Phys. **105**, 056101 (2009).
[25] S. Stathopoulos, L. Tsetseris, N. Pradhan, B. Colombeau, and D. Tsoukalas, J. Appl. Phys. **118**, 135710 (2015).
[26] G. Kresse and J. Furthmüller, Phys. Rev. B **54**, 11169 (1996).
[27] P. E. Blöchl, Phys. Rev. B **50**, 17953 (1994).
[28] H. J. Monkhorst and J. D. Pack, Phys. Rev. B **13**, 5188 (1976).
[29] J. P. Perdew, K. Burke, and M. Ernzerhof, Phys. Rev. Lett. **77**, 3865 (1996).
[30] W. H. Press, S. A. Teukolsky, W. T. Vetterling, and B. P. Flannery, *Numerical Recipes in C: The Art of Scientific Computing*, 2nd ed. (Cambridge University Press, 1992).
[31] G. Henkelman, A. Arnaldsson, and H. Jónsson, Comput. Mater. Sci. **36**, 354 (2006).
[32] S. L. Dudarev, G. A. Botton, S. Y. Savrasov, C. J. Humphreys, and A. P. Sutton, Phys. Rev. B **57**, 1505 (1998).
[33] H. Tahini, A. Chroneos, R. W. Grimes, and U. Schwingenschlögl, Appl. Phys. Lett. **99**, 162103 (2011).
[34] S. Grimme, J. Antony, S. Ehrlich, and H. Krieg, J. Chem. Phys. **132**, 154104 (2010).
[35] B. N. Dutta, Phys. Status Solidi B **2**, 984 (1962).
[36] A. Smakula and J. Kalnajs, Phys. Rev. **99**, 1737 (1955).
[37] M. T. Yin and M. L. Cohen, Phys. Rev. B **26**, 5668 (1982).
[38] C. Kittel, *Introduction to Solid State Physics*, 8th ed. (John Wiley & Sons, Hoboken, NJ, 2005).
[39] W. Bludau, A. Onton, and W. Heinke, J. Appl. Phys. **45**, 1846 (1974).
[40] S. M. Sze, *The Physics of Semiconductor Devices* (Wiley, New York, 2006).
[41] A. Dargys and J. Kundrotas, *Handbook on Physical Properties of Ge, Si, GaAs and InP* (Science and Encyclopedia Publishers, Vilnius, Lithuania, 1994).
[42] P. Yang, H.-K. Fun, I. A. Rahman, and M. I. Saleh, "Two phase refinements of the structures of α-Si_3N_4 and β-Si_3N_4 made from rice husk by Rietveld analysis," Ceram. Int. **21**, 137 (1995).
[43] R. Grün, "The crystal structure of β-Si_3N_4: Structural and stability considerations between α- and β-Si_3N_4," Acta Crystallogr., Sect. B: Struct. Crystallogr. Cryst. Chem. **35**, 800 (1979).
[44] S. N. Ruddlesden and P. Popper, "On the crystal structure of the nitrides of silicon and germanium," Acta Crystallogr. **11**, 465 (1958).
[45] S. Wild, P. Grieveson, and K. Jack, "The crystal structures of alpha and beta silicon and germanium nitrides," in *Special Ceramics* (British Ceramic Research Association, Stoke-on-Trent, UK, 1970).
[46] Z.-H. Yang, H. Peng, J. Sun, and J. P. Perdew, Phys. Rev. B **93**, 205205 (2016).
[47] M. Hu, Z. Wang, Y. Xu, J. Liang, J. Li, and X. Zhu, Phys. Chem. Chem. Phys. **20**, 26091 (2018).
[48] N. Kuganathan, H. Bracht, K. Davazoglou, F. Kipke, and A. Chroneos, AIP Adv. **11**(6), 065122 (2021).
[49] K. P. Huber and G. Herzberg, "Constants of diatomic molecules," in *Molecular Spectra and Molecular Structure* (Springer, Boston, MA, 1979).
[50] E. J. Little and M. M. Jones, J. Chem. Educ. **37**, 231 (1960).
[51] M. J. Puska, S. Pöykkö, M. Pesola, and R. M. Nieminen, Phys. Rev. B **58**(3), 1318 (1998).
[52] H. M. Pinto, J. Coutinho, V. J. B. Torres, S. Öberg, and P. R. Briddon, Mater. Sci. Semicond. Process. **9**(4), 498 (2006).